Appl. Phys. B 83, 87–91 (2006)
DOI: 10.1007/s00340-005-2118-5

**Applied Physics B**
**Lasers and Optics**

I. PELANT[1]
T. OSTATNICKÝ[2,*]
J. VALENTA[2,✉]
K. LUTEROVÁ[1]
E. SKOPALOVÁ[1]
T. MATES[1]
R.G. ELLIMAN[3]

# Waveguide cores containing silicon nanocrystals as active spectral filters for silicon-based photonics

[1] Institute of Physics, Academy of Sciences of the Czech Republic, 16253 Prague 6, Czech Republic
[2] Department of Chemical Physics & Optics, Faculty of Mathematics & Physics, Charles University, 121 16 Prague 2, Czech Republic
[3] Electronic Materials Engineering Department, Research School of Physical Sciences and Engineering, Australian National University, Canberra ACT 0200, Australia

**Received: 20 October 2005**
**Published online: 17 January 2006 •** **© Springer-Verlag 2005**

**ABSTRACT** Layers of densely packed luminescent Si nanocrystals embedded in fused silica act as wavelength-specific planar waveguides that filter the wide-band spontaneous emission. The waveguides' light output consists of two spectrally narrow ($\sim 10$ nm), orthogonally polarized, and spatially directed bands. This effect is shown to result from leaky modes of the lossy waveguides. The results have general applicability to lossy, asymmetric waveguides and show the way to produce spectrally narrow emission without the use of optical cavities.

**PACS** 78.67.Bf; 42.79.Gn; 81.07.Bc

## 1 Introduction

Silicon-based photonics is an exciting new area of research that aims to produce integrated electronic and photonic functionality in a single silicon chip. Silicon quantum dots or nanocrystals (Si-NCs) are efficient light emitters [1–3], unlike bulk silicon, and have been used to demonstrate silicon-based light-emitting diodes [4, 5]. The Si-NCs can also be employed to fabricate active optical waveguides [6–12]. Some of these Si-NC waveguides, with properly designed refractive-index profile, exhibit spectral filtering of the Si-NC photoluminescence emission. The filtered emission consists of narrow ($\sim 10$ nm), polarization-dependent emission lines [7, 8, 12]. This unexpected effect, which holds promise for potential applications in silicon photonics, was reported by Khriachtchev et al. [7] for $Si/SiO_2$ waveguides and by our group [12–14] (probably also by Ivanda et al. [15]) for samples containing Si-NC prepared by $Si^+$ implantation into silica slabs. Full understanding of the phenomenon is, however, still missing. Here we study this filtering effect in more detail and demonstrate, both experimentally and using theoretical modeling, that the origin of the filtering is based, contrary to intuition, on leaky modes of the lossy planar waveguides.

✉ Fax: +420-2-21911249, E-mail: jan.valenta@mff.cuni.cz
*Also at: IPCMS, Groupe d'Optique Nonlineaire et d'Optoelectronique, UMR 7504 CNRS-ULP, 67037 Strasbourg Cedex, France

## 2 Methods

The Si-NC thin-film waveguides were prepared by 400-keV $Si^+$-ion implantation into optically polished Infrasil slabs. Samples were subsequently annealed for 1 h at 1100 °C in a $N_2$ ambient to form Si-NCs and further annealed for 1 h at 500 °C in forming gas ($N_2/H_2$) to enhance the luminescence emission. The presence of Si-NCs and an estimate of their size was determined by Raman scattering, as shown in Fig. 1c. A simple approach, exploiting the shift and half-width of the Raman peak [16], provided an estimation of the Si-NC sizes from 4.4 nm to 5.9 nm.

Photoluminescence was measured at room temperature using a cw He-Cd laser (325 or 442 nm) and detected with a spectrograph coupled to a CCD camera. All spectra were corrected for the system response. Emitted light was coupled to the detection system either using a quartz optical fiber (collection angle $\sim 1°$) or by a microscope objective lens (magnification $\times 2.5$, NA $= 0.075$, collection angle $\sim 8.6°$). To measure a polar radiation diagram, the input of the optical fiber was rotated around the sample by a goniometer.

Phase-shift interferometry and atomic force microscopy (AFM) were used to characterize the surface morphology of the samples.

Neither spectral profiles nor spectral positions of substrate radiation modes can be calculated analytically. Numerical calculations were therefore performed using the formula for the cavity enhancement factor [17]. The relevant reflectivity coefficients on the boundaries were calculated using the transfer matrix method, taking into account the continuous profile of the refractive index. We also considered both the numerical aperture of the given experimental set-up and the loss coefficient in the Si-NC films. Details of this procedure will be published elsewhere.

## 3 Results and discussion

The visual appearance of our samples is shown in Fig. 1a. The refractive-index change for different implant fluences leads to variations in the color of the implanted regions under ambient (white) light. The resulting Si-NCs are embedded in the silica slabs as a thin ($\sim 1\,\mu$m) buried layer that

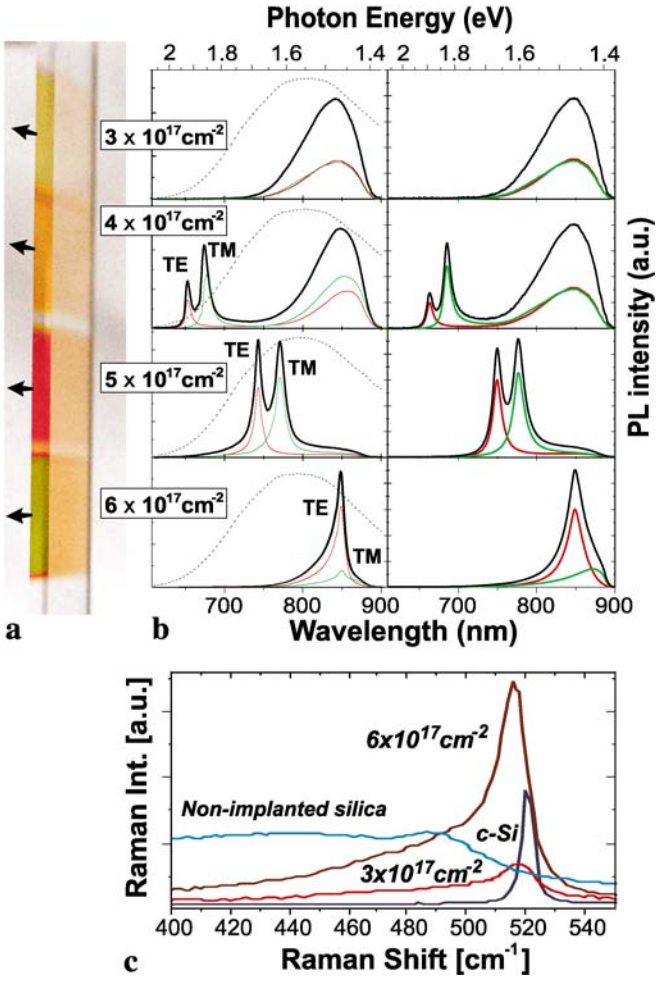


**FIGURE 1** Planar optical waveguides formed by Si-NC thin layers embedded in silica slabs. (**a**) Edge view of a silica sheet (Infrasil) $\sim 5.0 \times 1.0 \times 0.1\,\mathrm{cm}^3$ under diffused white light, with colored regions formed by Si-NC films. Corresponding implant fluences, ranging from 3 to $6 \times 10^{17}\ \mathrm{cm}^{-2}$, are indicated. (**b**) *Dotted curves*: conventional broad photoluminescence spectra from Si-NCs measured at normal incidence. *Full lines*: room-temperature photoluminescence spectra taken from the sample facet, in the direction indicated by *arrows* in (**a**). *Left-hand plots* – experimental, *right-hand plots* – calculated. (**c**) Examples of Raman spectra evidencing the presence of Si-NCs (*red* and *brown curves*). *Blue curve* – Raman spectrum of unimplanted Infrasil, *black curve* – reference spectrum of crystalline Si wafer

forms the high- refractive-index core of the waveguide structure. Because the refractive index of the Si-NC film is higher than that of the $SiO_2$ substrate and extends to the surface, the film acts as a planar asymmetric optical waveguide.

The effect of photoluminescence spectral filtering is highlighted in Fig. 1b. The left-hand column in this figure shows measured room-temperature photoluminescence spectra for four different Si-NC waveguides under UV excitation. The dotted curves represent emission from Si-NCs embedded within the waveguide core, measured from the sample surface, i.e. perpendicular to the Si-NC layer. Such broadband spectra are typical of the inhomogeneously broadened emission from Si-NCs but are undesirable for many optical applications. The solid curves represent spectra taken parallel to the surface, i.e. from the edge (facet) of the waveguide (arrows in Fig. 1a). The two sets of spectra are clearly quite different, the latter being composed of two distinct peaks separated by about 30 nm. Moreover, each of these peaks has a distinct linear polarization: the electric vector $\boldsymbol{E}$ of the short-wavelength peak lies in the Si-NC film (red curves, TE polarization) while the long-wavelength peak is characterized by $\boldsymbol{E}$ perpendicular to the film (green curves, TM polarization). The right-hand column in Fig. 1b represents theoretically calculated spectra, the basis of which will be discussed later.

The strong directionality of the TE/TM peak emission is highlighted in Fig. 2, which shows a polar radiation diagram of the spectrally integrated emission for the sample implanted to a fluence of $5 \times 10^{17}\ \mathrm{cm}^{-2}$. The emission contains surface Lambertian photoluminescence emission peaked at $\sim 90°$ (brownish areas in Fig. 2a), as well as two distinct lobes due to emission emanating from the sample edge (the left-hand lobe) and the internal reflection (the right-hand lobe). The well-developed TE/TM peaks occur within the left-hand lobe, close to the angle $\sim 0°$ only (yellow region in Fig. 2a). This is more clearly seen in Fig. 2b, where the photoluminescence emission was collected using a microscope objec-

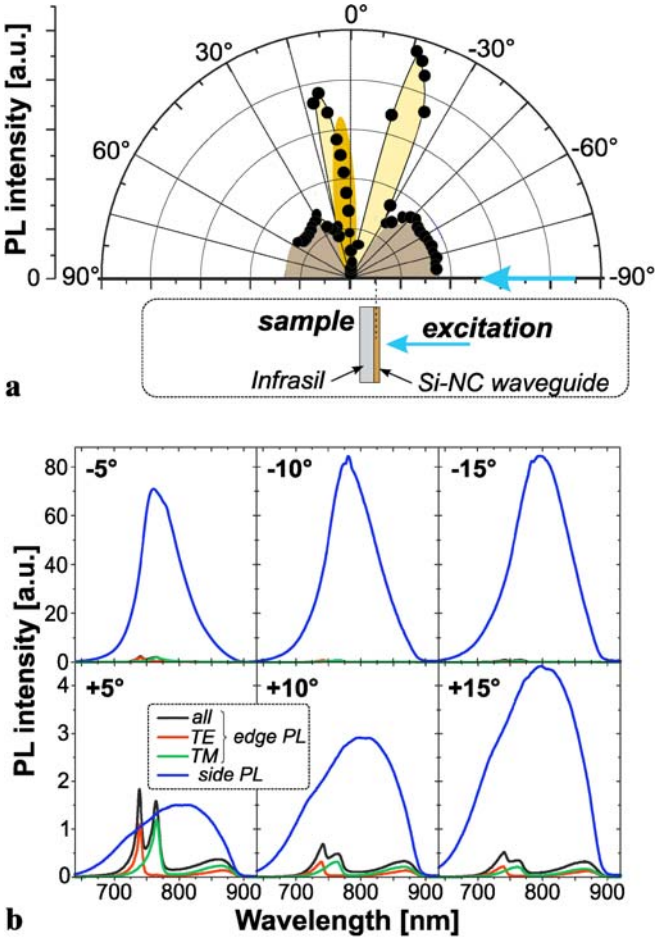


**FIGURE 2** Directionality of edge emission (the sample was implanted to a fluence of $5 \times 10^{17}\ \mathrm{cm}^{-2}$). (**a**) Spectrally integrated photoluminescence emission as a function of the polar angle, measured with the sample fixed at the center of a goniometer. (**b**) Micro-photoluminescence spectra for six directions ($\pm 5°, \pm 10°, \pm 15°$): the direct emission from the excited spot is plotted by *blue lines*, the edge emission by *black lines*, and the polarization-resolved TE and TM modes by *red* and *green lines*, respectively. (The collection angle of the objective lens is $\sim 8.6°$.) Note different intensity scales for *upper* and *lower* plots

tive (with numerical aperture of 0.075, i.e. collection angle of $\sim 8.6°$). The micro-imaging-spectroscopic set-up enabled us to detect separately photoluminescence leaving the excited spot directly (blue lines) and that coming from the edge of the implanted layer (black lines).

With regard to the physical processes that give rise to this novel spectral structure, we consider two distinct mechanisms (summarized in Fig. 3a and b):

(i) The two linearly polarized peaks could simply result from standard guided modes of the planar Si-NC waveguide (Fig. 3a). However, an ideal transparent planar waveguide should transmit a continuous spectrum of guided modes up to a cut-off wavelength [18]. The cut-off wavelength for the first-order modes of our waveguides can be estimated to lie above $\sim 1500$ nm. Consequently, the Si-NC films should transmit the entire 600–900 nm band emitted by the nanocrystals, which obviously is not the case. Nevertheless, some structure might arise from wavelength-dependent losses, with those modes (wavelengths) that undergo the smallest loss being guided to the edge of the sample. These are likely those modes that are 'weakly guided', i.e. the modes whose electric field is strongly delocalized, and the modes propagate basically as a planar wave in the substrate [18]. Their effective guide thickness tends to infinity [19]. Ray optics describes these modes by an angle of incidence $\theta$ that is greater than but very close to the critical angle $\theta_c$ for total internal reflection[1]. The situation is depicted in Fig. 3c, which displays schematically the reflectance $R$ and phase shift $\Phi$ of TE and TM waves on the boundary between two dielectric media as a function of $\theta$. In our case the boundaries are either the core/air (upper boundary) or the core/$SiO_2$ substrate (lower boundary). The arrow G labels the angle $\theta$ for the strongly delocalized guided modes, which were invoked [20, 21] to be responsible for the filtration effect. The salient feature of the filtering, namely, the separation between TE and TM modes, is then a direct consequence of the asymmetric guide. It is due to different phase shifts $\Phi$ for the TE and TM modes under total reflection at both boundaries. In order to fulfill the phase condition that after two successive reflections the phase difference can only be equal to an integral multiple of $2\pi$, suitable wavelengths from the (continuous) emission band are combined with available (continuous) values of $\Phi$. The latter is slightly different for TE and TM polarizations at a given angle of incidence (Fig. 3c) and results in mode wavelengths that are also slightly different.

(ii) The second possible mechanism involves substrate leaky or radiation modes of the Si-NC waveguide (Fig. 3b). These propagate at an angle $\theta$ situated close to but below $\theta_c$ (arrow S in Fig. 3c). These modes undergo total reflection at the upper boundary (larger index difference) but are only partially reflected on the lower boundary (smaller index difference). Consequently, a small fraction of their power is radiated into the substrate at each bottom reflection. These leaky modes are usually considered undesirable parasitic radiation [18] and thus do not normally receive much attention. If, however, the angle $\theta$ is only slightly less than $\theta_c$, the leaky modes propagate near-parallel to the Si-NC plane. Moreover, the number of reflections is very high ($R$ is close to unity), resulting in a narrow spectral width for the modes. The mechanism of spectral filtering in this case remains basically the same as discussed above, the only difference being that a phase shift $\Phi$ at the upper boundary only comes to play during the initial stages of propagation.

After a finite number of internal reflections all the radiant power escapes into leaky modes and emerges from the sample facet in a well-defined direction, basically parallel with the Si-NC film (see [14] and Fig. 2). This makes such leaky substrate modes virtually indistinguishable from the guided modes.

The fact that the two mechanisms have a different dependence on the refractive-index difference at the surface provides the basis for testing their validity. The principle is to change locally the cladding layer refractive index between a photoexcitation spot and the sample facet – which can be achieved by putting drops of various liquids on the sample surface close to the sample edge (Fig. 3a and b). If the effect of spectral filtering is due to weakly guided modes, then the edge-emission spectrum should be strongly distorted by such changes in index, since reflections on the upper boundary (now with modified refractive index) control the phase condition for mode creation all along the ray trajectory. If, on the other hand, the filtering is due to the substrate leaky modes, no change in the spectrum is expected since, after propagating $\leq 1$ mm from the excitation source, all energy flux in the modes has leaked into the substrate and is no longer influenced by the upper boundary (Fig. 3b).

Results of this experiment are displayed in Fig. 4a and show no change in emission spectrum for liquid refractive indices in the range from 1.359 to 1.657 – clear evidence that the effect is due to leaky substrate modes. (This ob-

[1] Here the lower boundary is of importance only since the refractive-index contrast at the upper boundary is high enough to assure total internal reflection at angles $\theta$ safely higher than $\theta_c$

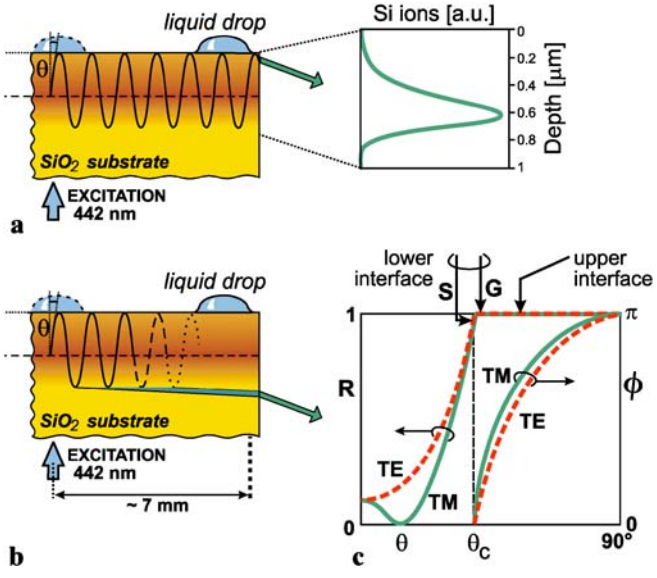


**FIGURE 3** Schematics of spectral filtering processes. (**a**) Guided modes of an asymmetric waveguide (*inset* shows implanted $Si^+$-ion distribution across the Si-NC film as calculated by SRIM (the Stopping and Range of Ions in Matter), which determines the refractive-index profile). (**b**) Substrate radiation (leaky) modes from the Si-NC core. (**c**) Reflectance and phase shifts on the planar boundary between two dielectric media plotted for TE and TM modes versus incident angle $\theta$

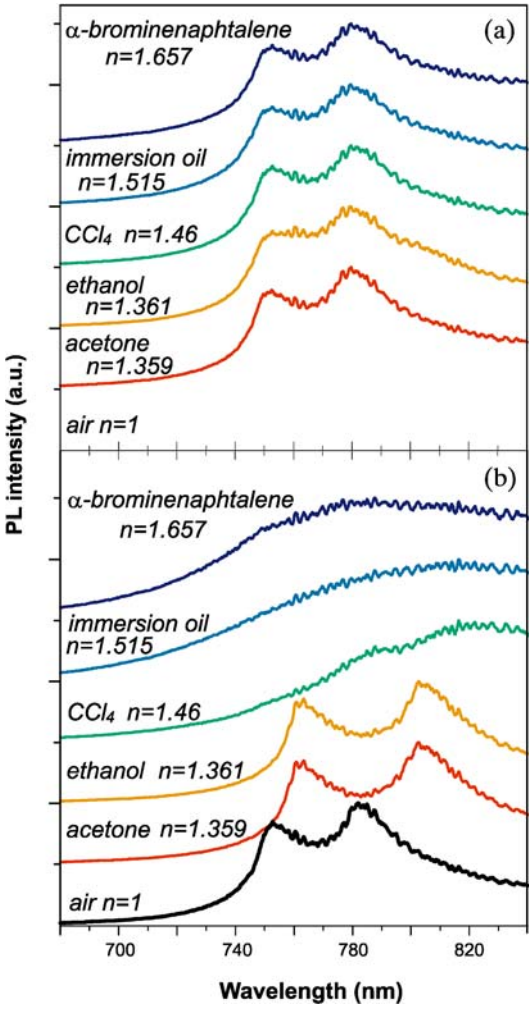


**FIGURE 4** Orthogonal polarization emission 'doublet' in the sample implanted to a fluence of $5 \times 10^{17}$ cm$^{-2}$. (**a**) Drops of various liquids located on the upper boundary between excitation spot and sample facet, as sketched by the *liquid drops* on the *right* in Fig. 3a and b. *Black curve* – blank upper boundary. (**b**) The same liquids as in (**a**) but located above the excitation spot (the *dotted drops* on the *left* in Fig. 3a and b)

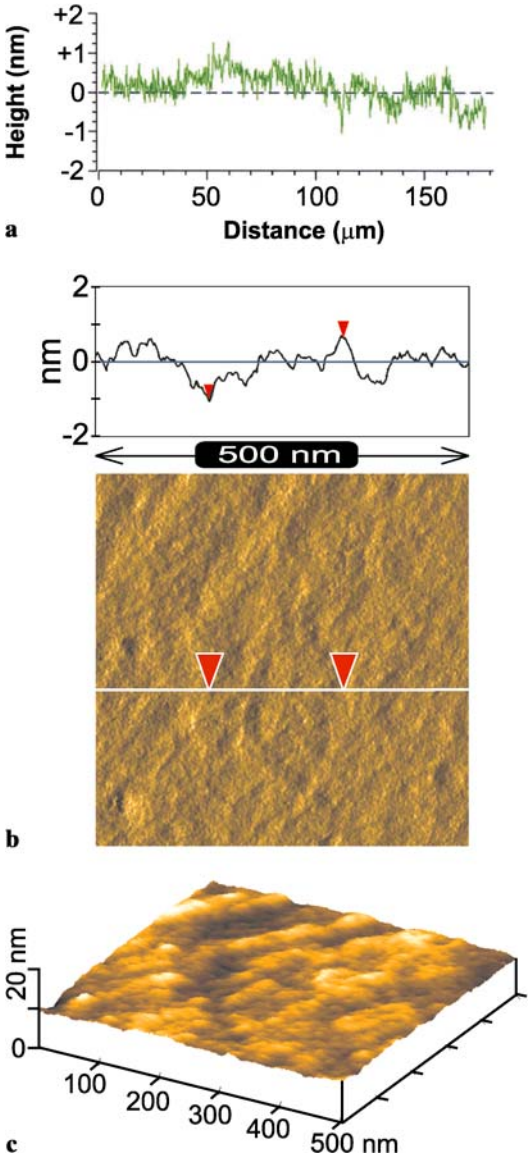


**FIGURE 5** Morphology of the sample surface (upper waveguide boundary). (**a**) Line profile measured with a ZYGO phase-shifting interferometer over a range of 180 μm. (**b**) AFM normal force image over an area of 500 × 500 nm$^2$. A selected line profile of the local height is also shown, giving the vertical distance between the points marked by *arrows* of about 1.7 nm, in good agreement with the interferometric data. (**c**) Three-dimensional image of the local height in a 500 × 500 nm$^2$ area. The $z$-range of the surface (minimum to maximum) is 3.9 nm, yielding a RMS roughness of 0.5 nm

servation contrasts with a similar experiment performed by shifting the same liquid drops just above the excitation spot – dotted drops in Fig. 3a and b – where reflections of the leaky modes on the upper boundary still occur. The results are shown in Fig. 4b: drastic spectral modifications, scaling with liquid refractive index [22].) As further confirmation of this model, the right-hand column in Fig. 1b shows theoretically calculated edge-emission spectra of the substrate radiation modes for all samples. In calculating these curves the graded index profile of each sample [14] was employed as extracted from interference-modulated optical transmission curves, measured in normal incidence[2]. It is evident that the calculated curves reproduce the measured spectra very well.

Importantly, the dominance of the leaky substrate mode emission implies the suppression of the broadband emission from the Si-NCs. (This latter emission is partly observed in samples implanted to fluences of $3 \times 10^{17}$ cm$^{-2}$ and $4 \times 10^{17}$ cm$^{-2}$ – Fig. 1b.) The attenuation of these guided modes is attributed to waveguide losses. Surface and side-wall roughness is often invoked to explain waveguide losses; however, this is not a likely cause in the present case. Indeed, in the present case the waveguide surface morphology (Fig. 5) is very flat with a RMS roughness of $\sim 0.5$ nm only. This value is substantially lower than typical side-wall roughness in e.g. etched semiconductor waveguides [23] or in typical silica waveguides [24]. The loss is therefore likely due to self-absorption and/or Mie scattering in the waveguide core. (Diffraction of the guided modes at the output facet may also play a role.) The exact nature of the observed waveguide attenuation remains unsolved at present.

[2] We take this opportunity to correct the original version of the calculated curves quoted in [14], where a numerical error made worse the agreement with experiment

## 4 Conclusions

To summarize, using a combination of experimental and theoretical results we have elucidated the principal role of substrate radiation modes in the spectral filtration effect of thin-film Si-NC waveguides. It is noteworthy that the narrow spectral width of both orthogonal polarization modes is comparable with the emission of Si-NCs in an optical microcavity [25, 26], without fabricating any Bragg reflectors. In a certain sense the investigated waveguides act as a microscopic Lummer–Gehrcke plate. The possibility of selecting the output wavelength via modification of waveguide parameters can be applicable in silicon photonics for Si-laser wavelength tuning, optical signal multiplexing, and optical sensing.

**ACKNOWLEDGEMENTS** Financial support through Research Grants Nos. 202/03/0789 and 202/01/D030 of GACR, Project No. IAA1010316 of GAAVCR, LC510 Centrum, and the Australian Research Council is greatly acknowledged. The research work at the Institute of Physics is supported by Institutional Research Plan No. AV0Z 10100521. The authors thank F. Trojánek for help with calculations and A. Poruba, A. Fejfar, and K. Kusova for experimental assistance.

## REFERENCES

1 G. Amato, C. Delerue, H.-J. von Bardeleben (eds.), *Structural and Optical Properties of Porous Silicon Nanostructures* (Gordon and Breach, Amsterdam 1997)
2 D.J. Lockwood (ed.), *Light Emission in Silicon. From Physics to Devices* (Semicond. Semimet. **49**) (Academic, San Diego, CA 1998)
3 S. Ossicini, L. Pavesi, F. Priolo (eds.), *Light Emitting Silicon for Microelectronics* (Springer Tracts Mod. Phys. **194**) (Springer, Berlin 2003)
4 A. Irrera, D. Pacifici, M. Miritello, G. Franzo, F. Priolo, F. Iacona, D. Sanfilippo, G. Di Stefano, P.G. Fallica, Appl. Phys. Lett. **81**, 1866 (2002)
5 R.J. Walters, G.I. Bourianoff, H.A. Atwater, Nat. Mater. **4**, 143 (2005)
6 L. Dal Negro, M. Cazzanelli, N. Daldosso, Z. Gaburro, L. Pavesi, F. Priolo, D. Pacifici, G. Franzo, F. Iacona, Physica E **16**, 297 (2003)
7 L. Khriachtchev, M. Räsänen, S. Novikov, J. Sinkkonen, Appl. Phys. Lett. **79**, 1249 (2001)
8 L. Khriachtchev, M. Räsänen, S. Novikov, J. Lahtinen, J. Appl. Phys. **95**, 7592 (2004)
9 J. Ruan, P.M. Fauchet, L. Dal Negro, M. Cazzanelli, L. Pavesi, Appl. Phys. Lett. **83**, 5479 (2003)
10 M. Cazzanelli, D. Navarro-Urrios, F. Riboli, N. Daldosso, L. Pavesi, J. Heitmann, L.X. Yi, R. Scholz, M. Zacharias, U. Gösele, J. Appl. Phys. **96**, 3164 (2004)
11 L. Pavesi, L. Dal Negro, C. Mazzoleni, G. Franzo, F. Priolo, Nature **408**, 440 (2000)
12 J. Valenta, I. Pelant, K. Luterová, R. Tomasiunas, S. Cheylan, R.G. Elliman, J. Linnros, B. Hönerlage, Appl. Phys. Lett. **82**, 955 (2003)
13 J. Valenta, I. Pelant, J. Linnros, Appl. Phys. Lett. **81**, 1396 (2002)
14 J. Valenta, T. Ostatnický, I. Pelant, R.G. Elliman, J. Linnros, B. Hönerlage, J. Appl. Phys. **96**, 5222 (2004)
15 M. Ivanda, U.V. Desnica, C.W. White, W. Kiefer, in *Towards the First Silicon Laser*, ed. by L. Pavesi, S. Gaponenko, L. Dal Negro (NATO Sci. Ser. II **93**) (Kluwer, Dordrecht 2003) pp. 191–196
16 G. Viera, S. Huet, L. Boufendi, J. Appl. Phys. **90**, 4175 (2001)
17 R. Baets, P. Bienstman, R. Bockstaele, in *Confined Photon Systems. Fundamentals and Applications*, ed. by H. Benisty, J.-M. Gerard, R. Houdre, J. Rarity, C. Weisbuch (Springer, Berlin 1999) pp. 39–79
18 H.G. Unger, *Planar Optical Waveguides and Fibres* (Clarendon, Oxford 1977)
19 H. Kogelnik, V. Ramaswamy, Appl. Opt. **13**, 1867 (1974)
20 L. Khriachtchev, M. Räsänen, S. Novikov, Appl. Phys. Lett. **83**, 3018 (2003)
21 L. Khriachtchev, S. Novikov, J. Lahtinen, M. Räsänen, J. Phys.: Condens. Matter **16**, 3219 (2004)
22 K. Luterova, E. Skopalova, I. Pelant, M. Rejman, T. Ostatnicky, J. Valenta, in preparation
23 J.H. Jang, W. Zhao, J.W. Bae, D. Selvanathan, S.L. Rommel, I. Adesida, A. Lepore, M. Kwakernaak, J.H. Abeles, Appl. Phys. Lett. **83**, 4116 (2003)
24 S. Janz, in *Silicon Photonics*, ed. by L. Pavesi, D.J. Lockwood (Springer, Berlin, 2004), pp. 323–360
25 S. Chan, P.M. Fauchet, Appl. Phys. Lett. **75**, 274 (1999)
26 F. Iacona, G. Franzo, E.C. Moreira, F. Priolo, J. Appl. Phys. **89**, 8354 (2001)